



A SERS nanocellulose-paper-based analytical device for ultrasensitive detection of Alzheimer's disease

Wenwen Yuan^{a,b,c}, Hang Yuan^a, Ruibing Li^d, Ruiqi Yong^a, Ivona Mitrovic^b, Eng Gee Lim^{a,b}, Sixuan Duan^{a,b,e}, Pengfei Song^{a,b,*}

^a School of Advanced Technology, Xi'an Jiaotong - Liverpool University, 215123, Suzhou, China

^b Department of Electrical Engineering and Electronics, University of Liverpool, L69 7ZX, Liverpool, UK

^c State Key Laboratory for Manufacturing Systems Engineering, Xi'an Jiaotong University, 710049, Xi'an, China

^d Department of Clinical Laboratory Medicine, The First Medical Centre, Chinese 301 General Hospital, 100853, Beijing, China

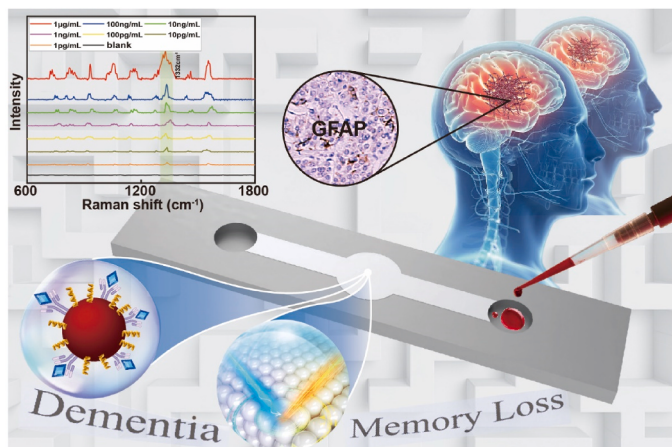
^e Key Laboratory of Bionic Engineering, Jilin University, 130022, Changchun, China



HIGHLIGHTS

- Ultrasensitive and low-cost detection of biomarker of Alzheimer's disease.
- Nanocellulose-paper-based biosensing microfluidic devices.
- Surface-enhanced Raman scattering immunoassay of GFAP.

GRAPHICAL ABSTRACT



ARTICLE INFO

Keywords:
Nanocellulose
Paper-based microfluidic device
Surface-enhanced Raman scattering
Alzheimer's disease
Immuno sensing

ABSTRACT

Background: Alzheimer's disease (AD), one of the most prevalent neurodegenerative diseases, results in severe cognitive decline and irreversible memory loss. Early detection of AD is significant to patients for personalized intervention since effective cure and treatment methods for AD are still lacking. Despite the severity of the disease, existing highly sensitive AD detection methods, including neuroimaging and brain deposit-positive lesion tests, are not suitable for screening purposes due to their high cost and complicated operation. Therefore, these methods are unsuitable for early detection, especially in low-resource settings. Although regular paper-based microfluidics are cost-efficient for AD detection, they are restricted by a poor limit of detection (LOD).

* Corresponding author. School of Advanced Technology, Xi'an Jiaotong - Liverpool University, 215123, Suzhou, China.
E-mail address: Pengfei.Song@xjtu.edu.cn (P. Song).

Results: To address the above limitations, we report the ultrasensitive and low-cost nanocellulose paper (nanopaper)-based analytical microfluidic devices (NanoPADs) for detecting one of the promising AD blood biomarkers (glial fibrillary acidic protein, GFAP) using Surface-enhanced Raman scattering (SERS) immunoassay. Nanopaper offers advantages as a SERS substrate, such as an ultrasmooth surface, high optical transparency, and tunable chemical properties. We detected the target GFAP in artificial serum, achieving a LOD of 150 fg mL^{-1} . **Significance:** The developed NanoPADs are distinguished by their cost-efficiency and ease of implementation, presenting a promising avenue for effective early detection of AD's GFAP biomarker with ultrahigh sensitivity. More importantly, our work provides the experimental routes for SERS-based immunoassay of biomarkers on NanoPADs for various diseases in the future.

1. Introduction

Alzheimer's disease (AD) is a severe neurodegenerative disease that leads to profound cognitive decline and memory impairment [1–3]. AD has been becoming an increasingly serious social and health issue with the aging of the population [4]. Growing research has shown that accurate diagnosis of AD is challenging due to the variability in dementia pathology and individual physiological variances among patients [5]. While neuropsychological cognitive tests and brain imaging are currently used in the early detection of AD, the limited reliability of cognitive testing and the high cost of brain imaging often lead to late diagnosis or misdiagnosis [6,7]. The biomarker-based early detection of AD, with clear diagnostic separation from other neurodegenerative diseases, is essential to prevent dementia and reduce social burdens [8]. It has been demonstrated that reactive astrogliosis, a complex and dynamic response to AD, involves the overexpression of glial fibrillary acidic protein (GFAP) by reactive astrocytes under pathological conditions [9]. Notably, the concentration of GFAP in human serum has been proven to be effective for the identification of AD in its early stages [10–12]. However, the traditional assays for detecting GFAP, such as enzyme-linked immunosorbent assay (ELISA), fluorescent immunoassay, and electrochemistry, typically involve cumbersome procedures, long reaction times, and large sample quantities, among others [13,14]. Therefore, it is essential to develop an ultra-sensitive and rapid GFAP detection technique for early identification of AD.

Recently, nanofibrillated cellulose (NFC) paper (nanopaper) has been emerging as a highly promising substrate material for various applications, including flexible electronics, biomedical devices and among others [15–19]. Like traditional paper, nanopaper is environmentally friendly, low-cost, biocompatible, and of a biodegradable nature since it can be obtained from plants [20,21]. In the context of surface-enhanced Raman scattering (SERS), nanopaper possesses unique characteristics that can enhance sensitivity. First, nanopaper serves as an excellent substrate material for optical sensors due to its high optical transparency (over 95% transmittance in the wavelength range of 350–800 nm), which can reduce the optical loss of the substrate [22,23]. Second, it exhibits an ultrasmooth surface with a roughness of less than 25 nm and dense cellulose matrix structures [19,24]. These characteristics of nanopaper facilitate the construction of highly organized and uniform nanostructures, thereby enhancing the tunability and stability of nanopaper-based devices [25,26]. Third, nanopaper has various functional groups (including carboxyl and hydroxyl groups) and can easily generate *in-situ* SERS plasmon without complicated functionalization on its surface. Otherwise, compared to other SERS substrates such as glass and PDMS, nanopaper does not necessitate complex pretreatment, including strong acid treatment, thanks to its various surface functional groups [27]. In our previous work, we developed a nanopaper-based SERS multiwell plate, achieving a femtomole limit of detection (LOD) for Rhodamine B [28]. Furthermore, we designed a facile micro-embossing technique that is low-cost, highly sensitive, ease-of-operation, enabling the fabrication of microchannels on nanopaper. This technique has been employed to develop and demonstrate nanopaper-based analytical microfluidic devices (NanoPADs) for SERS detection [25]. NanoPADs provide integrated growth of plasmon

through a simple ion layer absorption-reaction process and realize ultrahigh enhancement factor (1.34×10^9). Another advantage of the NanoPADs compared to other substrates is that the reaction zone of NanoPADs has a cover layer and can avoid contamination during reaction and detection processes. To date, nanopaper has shown great interest as a SERS substrate with high sensitivity, and user-friendly NanoPADs can provide an excellent platform for SERS detection. However, nanopaper-based devices for SERS immunoassay have not been developed yet.

In this paper, we report the ultrasensitive and low-cost SERS bio-sensing NanoPADs. Compared to the existing methods, our platform offers ease-of-operation and eliminates the need for intricate fabrication. Gold nanoparticles (AuNPs) were selected as SERS tags due to their high signal produced by wavelength, geometric anisotropy and surface plasmon resonance coupling [29,30]. Additionally, we employed 5, 5'-Dithiobis-2-nitrobenzoic acid (DTNB) to enhance the Raman signal of the SERS tags [31,32]. The SERS substrate was fabricated using *in-situ* grown silver nanoparticles (AgNPs) through the ion layer absorption and reaction process. To verify the feasibility of our experimental design, we initially detected rabbit IgG antigens with the LOD as low as 369 fg mL^{-1} . Subsequently, we detected the target AD biomarker (GFAP) in artificial serum, achieving a LOD of 150 fg mL^{-1} . Our method provides a new and practical approach for rapidly diagnosing AD complications with high sensitivity and selectivity, compared to the LOD of immunoassay on the traditional papers [33] and other transparency substrates (glass) [34]. The selectivity and specificity experiments were also performed, and it shows our method can effectively avoid interference from other AD markers (i.e., alkaline phosphorylation tau (P-tau) and β -Amyloid protein 42 ($A\beta$ 42)) and exhibit good specificity. Furthermore, it provides a cost-efficient method for monitoring AD deterioration risks, contributing to the prevention of long-term effects and reducing the incidence rate.

2. Methods

2.1. Reagents and materials

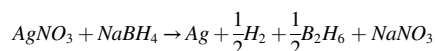
The (2,2,6,6-tetramethylpiperidin-1-yl)oxyl (TEMPO)-oxidized NFC slurry (1.0 wt% solid, carboxylate level 2.0 mmol/g solid, average nanofiber diameter: 10 nm) was purchased from Tianjin University of Science and Technology (Tianjin, China). DTNB (>98%) and Phosphate Buffer (PB) ($\text{KH}_2\text{PO}_4/\text{Na}_2\text{HPO}_4$, 0.5 M, pH = 7.0) were obtained from Macklin (Shanghai, China). $\text{HAuCl}_4 \cdot 3\text{H}_2\text{O}$ (>99.9%), NaBH_4 (>98%), $\text{K}_3\text{Fe}(\text{CN})_6$ (>99%), $\text{K}_4\text{Fe}(\text{CN})_6$ (>99.9%), KCl (>99.8%) and sodium citrate (>98%) were purchased from Aladdin (Shanghai, China). AgNO_3 (>99%) was ordered from Hushi (Shanghai, China). Mercaptopropyl-triethoxysilane (MPTES) (>95%) was bought from TCI (Shanghai, China). Rabbit IgG, IgG antibodies, Tween 20 (50% solution) and bovine serum albumin (BSA) were purchased from Sigma (U.S.A.). Recombinant human GFAP protein and anti-GFAP antibodies were bought from Abcam (U.K.). P-tau and $A\beta$ 42 were obtained from Bioss (Beijing, China). Artificial serum was ordered from Huzhou Inno Reagents Biotechnology Co., Ltd. (Zhejiang, China).

2.2. Preparation of the SERS substrates

The 4.0 g TEMPO-oxidized NFC slurry was dispersed in distilled water to a final content of 0.1 wt%, and the suspension was stirred until fully mixed. The above prepared suspension was vacuum filtered with a polyvinylidene difluoride (PVDF) filter membrane (VVLPO4700, EMD Millipore Corporation, pore size: 0.1 μm) on a glass filter holder to have a wet transparent nanopaper gel. For the preparation of Teflon molds, we first designed the mold layout by AutoCAD 2019 (Autodesk, San Rafael, CA) and then used a laser cutting machine (Han's Yuming Laser CMA0604-B-A, China) to cut the Teflon membrane. The cut Teflon molds were placed on the filtered nanopaper gel between two poly(ethylene terephthalate) films for hot embossing at 75 °C and 750 kPa for 10 mins. After releasing the Teflon molds, an additional layer of nanopaper gel was bonded spontaneously in the drying oven by nanofiber diffusion at 75 °C for around 1 h (Fig. 1a).

Due to the high molar extinction coefficient and excellent optical properties, AgNPs were widely used as SERS substrates [35,36]. An *in-situ* approach was used to grow AgNPs directly in the detection zone of NanoPADs, where highly structured and dense AgNP arrays can achieve high-sensitivity SERS sensing. Fig. S1 shows the SERS-based NanoPADs design, which consists of two microchannels that meet in the detection zone (labeled circular area in Fig. S1). The *in-situ* method was based on the simple ion layer adsorption and reaction process [37,38]. In short, silver ions were used to replace the positive ions on the carboxyl group of the reaction zone, and then BH_4^- was used to reduce Ag^+ on the surface of the nanopaper (Fig. S1) [39,40]. The chemical

reactions involved in the process are represented by the following formula [41]:



AgNO_3 and NaBH_4 were used as silver precursors and reducing agents, respectively.

For the purpose of preventing contamination and generating *in-situ* AgNPs, our developed NanoPADs have two inlet zones for adding AgNO_3 and NaBH_4 , respectively. This design can ensure that AgNPs are generated in the inlet zone instead of the reaction zone. The SERS tags can flow in from the outlet zone to fully integrate AgNPs in the reaction zone rather than in the two inlet channels. In brief, 5 μL of the 20 mM AgNO_3 was dropped in the left inlet zone of the channel and preserved in the reaction zone for 30 s. The abovementioned procedure was repeated five times to ensure a uniform distribution of AgNPs without agglomeration. 5 μL distilled water was dropped in the outlet zone for washing. Then, 5 μL of the 20 mM NaBH_4 was added to the right inlet zone to avoid contamination for utilizing AgNPs. 5 μL distilled water was dropped in the outlet inlet zone for washing (Fig. S1).

2.3. Preparation of AuNPs

According to the reported methods [42,43], first, 188.5 mL HAuCl_4 (0.04%) aqueous solution was prepared, injected into a flat-bottomed flask equipped with a magnetic stirrer, and heated to boiling. Second, 11.5 mL $\text{C}_6\text{H}_5\text{Na}_3\text{O}_7 \cdot 2\text{H}_2\text{O}$ (1%) was added to the flask under the

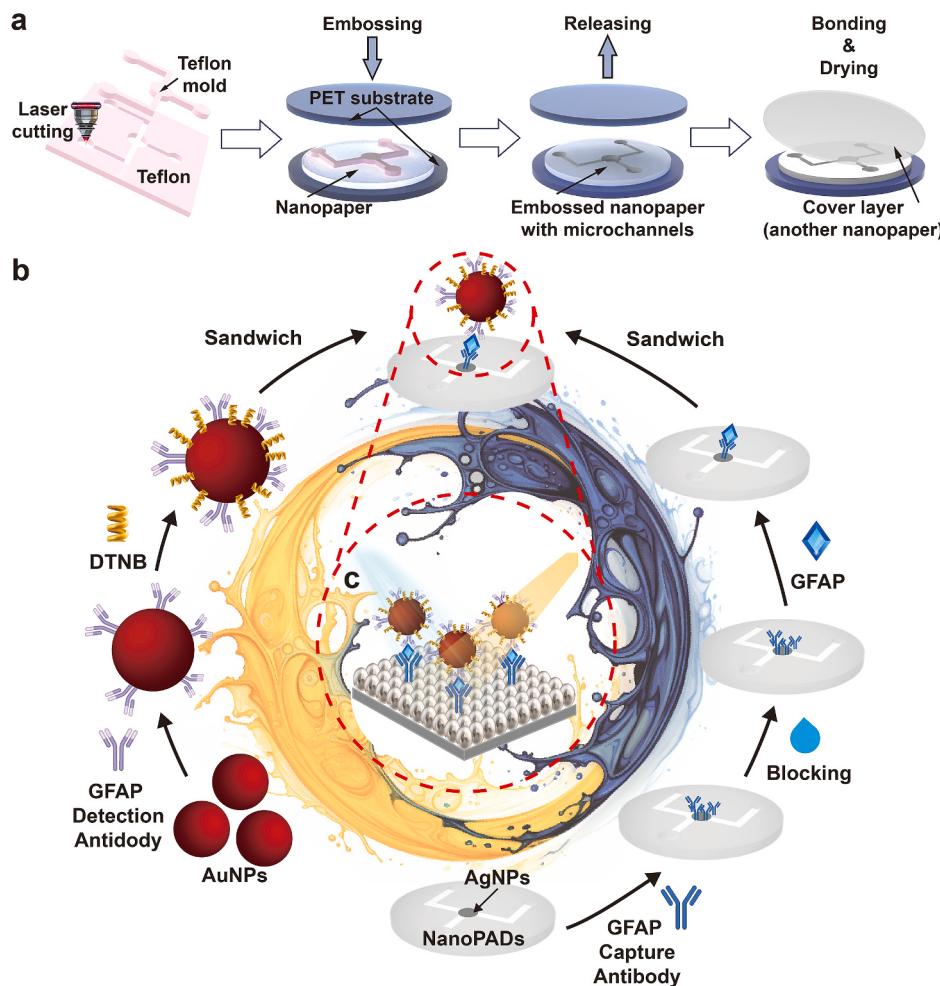


Fig. 1. Schematic of SERS detection. (a) Schematic of NanoPADs fabrication. (b) Preparatory illustration of SERS-based immunoassay for detecting the AD biomarker GFAP. (c) Schematic of SERS-based immunoassay.

diversion of a glass rod and continued heating under strong stirring. The color of the solution gradually changes from colorless and transparent to black, then mauve, and finally to dark red. The solution was heated and stirred until the color no longer changed, and the heating was stopped to produce AuNPs. After cooling to room temperature, AuNPs were stored in a refrigerator at 4 °C for later use.

2.4. Fabrication of DTNB-labeled SERS tags

In this work, DTNB, a highly Raman-active molecule, was employed as a Raman reporter co-immobilized on AuNPs, and successfully introduced to improve the sensitivity. The intensity has reached the orders of more than 10 times compared with label-free SERS detection [44]. First, GFAP detection antibody solution (100 µg mL⁻¹ in 0.1 M PB, pH = 7.0) was slowly added to the equivalent suspension of AuNPs (1 mL) under 4 °C for 1 h. By interacting between ionic, and hydrophilic and hydrophobic mercaptan groups, GFAP detection antibody was adsorbed onto AuNPs [45–49]. After centrifugation at 10000 rpm for 1 h at 4 °C, free antibodies were removed, and BSA (1% of 0.1 M PB) was added to the residual complex to seal the unmodified part of the surface of AuNPs and centrifuged again (at 10000 rpm for 1 h at 4 °C). Then, anti-GFAP@AuNPs were resuspended in 1 mL of PB (0.1 M, pH = 7.0) solution. 1 mL DTNB solution (1 mM in 0.1 mM PB, pH = 8.5) was added to the above anti-GFAP@AuNPs solution and kept stirring for 1 h at 4 °C. After interacting with AuNPs, DTNB was divided into two parts and spontaneously fixed on the surface of AuNPs by mercaptan groups. After centrifugation at 10000 rpm at 4 °C for 1 h, SERS tags were resuspended in 1 mL of PB and can be stored for 1 month under 4 °C. The fabrication of IgG SERS tags follows the same chemical route.

2.5. Immunoassay protocol

The SERS-based immunoassay was conducted using a standard sandwich ELISA method. The working principle of the proposed strategy for AD biomarker GFAP is shown in Fig. 1b. First, the GFAP capture antibody was fixed on the AgNPs surface to form a uniform antibody layer on the reaction pore. 20 µL capture antibody solution (100 µg mL⁻¹ in 0.1 M PB, pH = 7.0) was pipetted into the inlet zone of the NanoPADs. The immobilization was carried out at 37 °C for 2 h to coat the antibody on the NanoPADs substrate. The washing solution (0.05% Tween 20 in 0.1 M PB) was used to wash and remove the residual antibody for three times. Then, a well-blocking solution fully blocked the substrate (2% BSA in 0.1 M PB, pH = 7.0) at 37 °C for 2 h. The reacted substrate was rinsed thoroughly and stored at 4 °C for 1 month under protection.

The concentration range of the GFAP antigen solution was determined by continuous dilution with PB and artificial serum, ranging from 1 µg mL⁻¹ to 1 pg mL⁻¹, respectively. 20 µL GFAP antigen solution was added and transferred into the inlet zone of the NanoPADs on the antibody immobilization substrate and incubated at 37 °C for 2 h. The washing solution was used to wash and remove the residual protein for three times. 50 µL DTNB@anti-GFAP@AuNPs suspension was further incubated at 37 °C for 2 h in the NanoPADs. All samples were thoroughly washed and stored at 4 °C before the SERS detection. Fig. 1c shows the prepared NanoPADs used for SERS-based immunoassay. The immunoassay protocol of IgG follows the same chemical route.

2.6. SERS measurement

All Raman spectra were measured by Horiba XploRA (Japan) under 532 nm with a 50 × objective. IgG or GFAP antigen solution was determined by continuous dilution with PB and artificial serum, ranging from 1 µg mL⁻¹ to 1 pg mL⁻¹, respectively. The Raman spectra were acquired in the region of 600–1800 cm⁻¹ with a spectral resolution of 2 cm⁻¹, and the laser intensity was set as 0.1% with the least noise. Raman spectra were taken from the average of seven measurements. All spectral data was analyzed using Origin lab software. A baseline correction

procedure was performed to obtain the final spectrum for each measurement.

2.7. Electrochemical impedance spectroscopy (EIS) characterization of DTNB@anti-GFAP@AuNPs SERS tags

50 µL of AuNPs, anti-GFAP@AuNPs and DTNB@anti-GFAP@AuNPs solutions were dropped on thiolated Indium Tin Oxide (ITO) glass contained by MPTES. The glass can form a stable Au-S bond by modification so that analytes can be stably modified on the ITO surface. A three-electrode system was chosen for the experiment: a modified electrode with AuNPs, anti-GFAP@AuNPs and DTNB@anti-GFAP@AuNPs as the working electrode, a platinum wire electrode as the counter electrode, and a saturated calomel electrode as the reference electrode. The electrochemical impedance investigation was performed using a 0.1 M KCl solution containing 0.1 M K₄[Fe(CN)₆] and 0.1 M K₃[Fe(CN)₆]. EIS was performed using an electrochemical workstation (Metrohm PGSTAT302 N, Switzerland) with an initial potential of 0.1 V, spanning a frequency range from 10⁻¹ to 10⁵ Hz.

2.8. Instrumentation

The formation of prepared AuNPs and DTNB@anti-GFAP@AuNPs was monitored during the preparation process by UV-vis spectrophotometer (Agilent Cary 60, U.S.A.).

Transmission electron microscopy (TEM) images were obtained with transmission electron microscopy at 50 kV accelerating voltage (FEI Talos F200X G2, U.S.A.).

Scanning electron microscope (SEM) (FEI Scios 2 HiVac, USA) was used to characterize the morphology of AgNPs at a working voltage of 5 kV.

Fourier transform infrared spectrometer (FTIR) (Thermo Scientific, iS50, U.S.A.) was used to characterize the coating of protein on AuNPs.

All spectral data was analyzed using Origin 2022 (OriginLab, U.S.A.). A baseline correction procedure was performed to obtain the final spectrum for each measurement.

3. Results and discussions

3.1. Characterization

To confirm the adsorption of GFAP detection antibody onto the surface of AuNPs, several characterizations were demonstrated. First, various concentrations of GFAP were introduced, and the corresponding UV-vis adsorption spectra were measured. The protein will adhere to and bind with the AuNPs surface through strong ion interactions, as well as form the thiol-Au link upon combining the protein and AuNPs solution [50]. Consequently, its characteristic peak can be detected by UV-vis. Fig. 2a depicts the UV-vis adsorption spectral responses of bare AuNPs and incubated anti-GFAP@AuNPs with different concentrations of GFAP antibodies. Using the spectrum of the bare AuNPs as a control, the increase in GFAP antibody concentration led to a gradual reduction in the adsorption intensity, indicative of the consumption of individual AuNPs. However, no significant aggregation occurred as the GFAP antibody concentration ranged from 20 to 200 µg mL⁻¹. Contrary to nonspecific contacts or instability, the aggregation of nanoconjugates was prompted by specific recognition of the target protein. Fig. 2a demonstrates a prominent surface plasmon resonance (SPR) adsorption peak at 528 nm, which is characteristic of individual AuNPs. Notably, the anti-GFAP@AuNPs conjugates displayed a comparable SPR peak (532 nm) with a red shift of 5 nm, indicating the successful capping of GFAP block oligonucleotides on the surface of AuNPs [51]. Furthermore, Fig. S2 illustrates the UV-vis spectra of DTNB@anti-GFAP@AuNPs, and the characteristic peak is around 538 nm. This indicates that the average size of the particles is approximately 54 nm, providing evidence that supports the successful preparation of SERS tags.

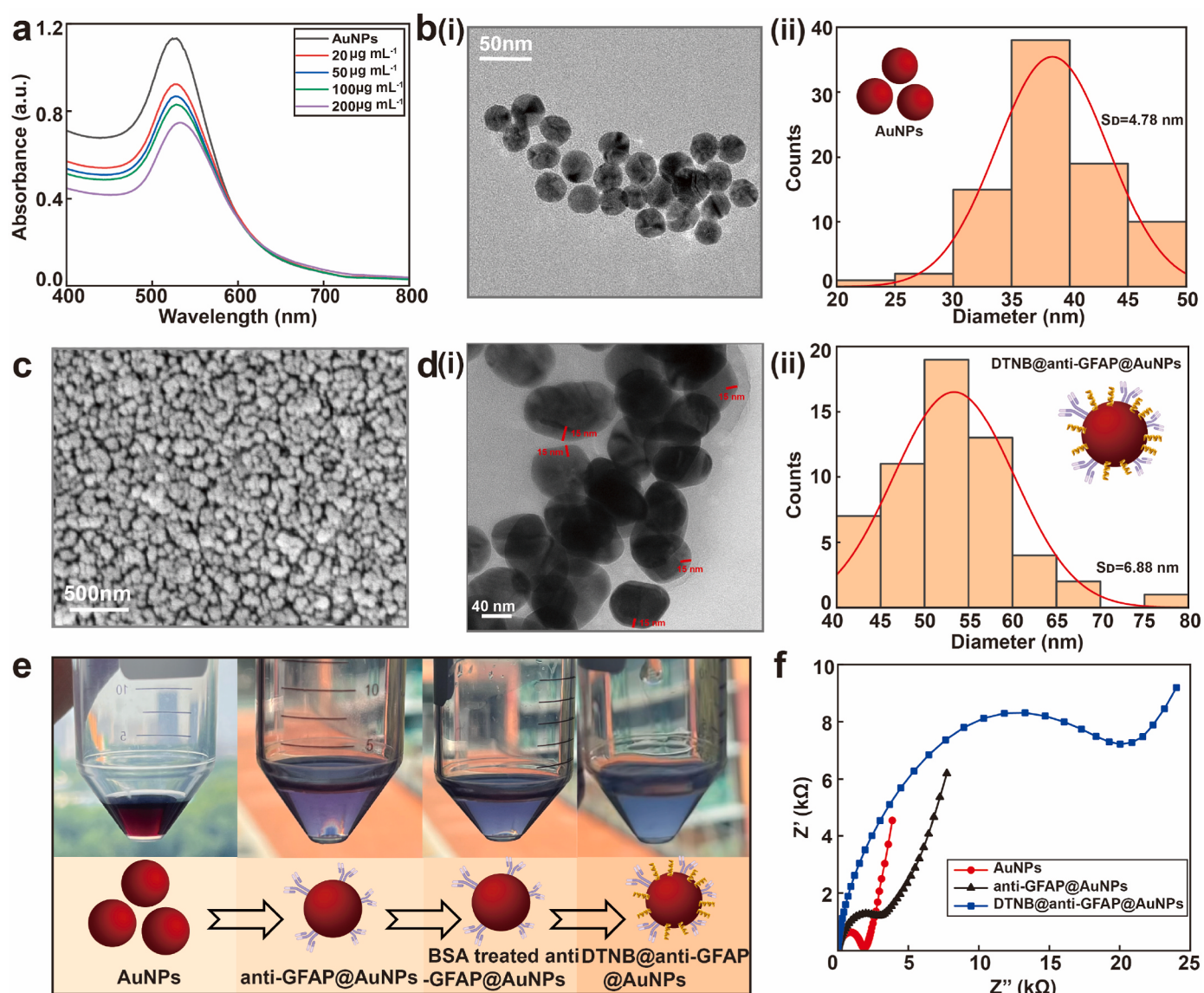


Fig. 2. Characterization of AuNPs SERS tags. (a) UV-vis absorption spectra of bare AuNPs and anti-GFAP@AuNPs at different concentrations of GFAP antibody. (b) (i) TEM image and (ii) size distributions of AuNPs. (c) SEM image of *in-situ* AgNP substrate. (d) (i) TEM image and (ii) size distributions of DTNB@anti-GFAP@AuNPs. (e) Photographs of the color change during the SERS tags fabrication process. (f) Electrochemical characterization of the SERS tag preparation process. (For interpretation of the references to color in this figure legend, the reader is referred to the Web version of this article.)

DTNB@anti-GFAP@AuNPs SERS tags were synthesized using a two-step method involving UV-vis adsorption and TEM characterization. Typical TEM images of AuNPs and detailed DTNB@anti-GFAP@AuNPs are presented in Fig. 2b(i) and 2d(i), revealing their spherical shape and uniform size. The prepared AuNPs, displayed in Fig. 2b, exhibited uniformity, monodispersity, and suitability for SERS tag fabrication. Uniform and well-organized AuNP arrays were formed, boasting a relatively smooth surface and an average diameter of 40 ± 4.78 nm. Following protein coating, the DTNB-labeled AuNPs aggregates exhibited an average protein thickness of 14 nm and an average total diameter of approximately 54 ± 6.88 nm. This variation in hydrodynamic diameter is derived from the adsorbed layer of DTNB@anti-GFAP. Size distributions of the bare AuNPs and the DTNB@anti-GFAP@AuNPs SERS tags are illustrated in Fig. 2b(ii) and 2d(ii), affirming the stability of the synthesized nanoconjugates. The TEM photo of anti-GFAP@AuNPs is illustrated in Fig. S6. TEM photos conclusively verified the successful creation of core-satellite sandwich structures during the fabrication process.

Fig. 2e displays the photographs illustrating the color change

dependent on ionic strength throughout the process. It is evident that the suspension turned blue as more molecules were absorbed during the fabrication process. These photographs visually confirm the successful generation of DTNB@anti-GFAP@AuNPs SERS tags.

EIS stands as an effective method to probe the characteristics of a surface-modified electrode. The electron transfer resistance, governing the kinetics of electron transfer for the redox probe on the electrode surface, is manifested as the semicircle diameter in the EIS plot. As depicted in Fig. 2f, the complex impedance plots for variously layered modified electrodes are presented. The modified protein and DTNB limited electrochemical activity, which impeded electron transport between the $[\text{Fe}(\text{CN})_6]^{3-/-4-}$ solution and the electrode, resulting in the evident attenuation of redox peaks. This spectral evidence unequivocally verified the successful integration of DTNB@anti-GFAP@AuNPs SERS tags.

FTIR is instrumental in identifying biomolecules and Raman reporters involved in the synthesis of gold-labeled probes by analyzing specific spectral features. An identification-signaling molecular fingerprint is produced when infrared radiation is applied to synthetic AuNPs

[52]. The radiation enters the solution containing the synthesized AuNPs and is partially absorbed, with the remaining radiation passing through the material. As shown in Fig. S3, amide bands present in the anti-GFAP@AuNPs FTIR spectrum at 1525 cm^{-1} (N–H bending and C–N vibrations), 1651 cm^{-1} (C=O stretching of amide bands), 3400 cm^{-1} (N–H stretching), which illustrates the successful coating of GFAP [53]. The coating of DTNB was proved by the N=C=S stretching at 2008 cm^{-1} , while DTNB and proteins will form the aforementioned bond [54]. The results of FTIR indicate the successful generation of anti-GFAP@AuNPs and DTNB@anti-GFAP@AuNPs SERS tags.

The well-growing SERS platform also significantly contributes to achieving highly sensitive detection. As depicted in Fig. 2c, a photograph of the NanoPADs featuring *in-situ* grown AgNPs highlights its readiness for testing. The AgNPs were further characterized through SEM imaging, revealing the formation of dense, uniform, and well-organized AgNPs arrays with an average diameter of $55.37 \pm 6.7\text{ nm}$ ($n = 100$). These characteristics pave the way for enhanced Raman signals, as serum coupling produces numerous hotspots. The application of a monolayer of AgNPs serves as an excellent substrate for antibody collection in the suggested sandwich SERS immunoassay.

3.2. SERS of DTNB-labeled immunogold nanoparticles

The electronic bilayer around AuNPs induced by the initially adsorbed stabilizer may be disturbed by the SERS reporter and lead to AuNPs precipitation. 1 mM DTNB solution was slowly mixed with an equal volume of AuNPs solution to prevent the instability of AuNPs. In addition, $20\text{ }\mu\text{L}$ of the 1 mM DTNB analyte solution was dropped on the inlet zone of the channel of NanoPADs and dried to detect the SERS activity in the reaction zone. Fig. 3a and b show the Raman spectra of the DTNB synthesized on NanoPADs and AuNPs, respectively. The pure Raman spectrum of DTNB is characterized by peaks at 1333 cm^{-1} , 1067 cm^{-1} , 1152 cm^{-1} , and 1558 cm^{-1} , attributed to the symmetric nitro group stretch, succinimidyl N–C–O stretch overlapping with aromatic ring modes, C–H deformation modes, and the aromatic ring C–C stretching modes, respectively [55]. The characteristic peak of DTNB at 1333 cm^{-1} (Fig. 3b) is significantly enhanced by the DTNB-AuNPs interaction facilitated by neighboring molecules [55]. Fig. 3c shows the SERS spectrum of the prepared IgG@AuNPs. The Raman peaks of pure IgG protein at 1366 cm^{-1} , 1511 cm^{-1} , 1574 cm^{-1} and 1649 cm^{-1} indicate the stretching of tryptophan v-ring, and the peaks at 1511 cm^{-1} and 1574 cm^{-1} also indicate the stretching of tyrosine v-ring [56]. These peaks correspond to characteristic Raman-active amino acids in IgG sequences. The peak at 1632 cm^{-1} is attributed to amide overlapping with water. Upon adding the DTNB solution to the IgG@AuNPs solution, the SERS signal of DTNB takes precedence (Fig. 3d). The comparison of Fig. 3b and d reveals certain peaks shift upon combining DTNB@IgG@AuNPs, unlike those in the combination of DTNB@AuNPs. These shifts may arise from changes in the distance between the molecule and the AuNPs surface, resulting in alterations in the electromagnetic or chemical enhancement effects of SERS [44]. Detection sensitivity can be enhanced by targeting the Raman reporter rather than directly detecting IgG. Notably, Raman reporter DTNB's sensitivity is 5 times greater than that of IgG (Fig. 3c vs. Fig. 3d). The SERS sandwich result of IgG protein on NanoPADs is shown in Fig. 3e. The intensity of Raman signal on NanoPADs was higher than the result of DTNB@IgG@AuNPs. While maintaining the same selectivity as traditional sandwich immunoassays, the SERS method employs Raman-active reporter molecules like DTNB. The presented results affirm the substrate's stability, rendering it suitable for subsequent experiments.

3.3. Feasibility of rabbit IgG SERS detection

Fig. 4a displays the SERS spectra of DTNB@anti-IgG@AuNPs captured by rabbit IgG at varying concentrations (from $1\text{ }\mu\text{g mL}^{-1}$ to $1\text{ }\mu\text{g mL}^{-1}$). The intensity of SERS bands corresponding to DTNB

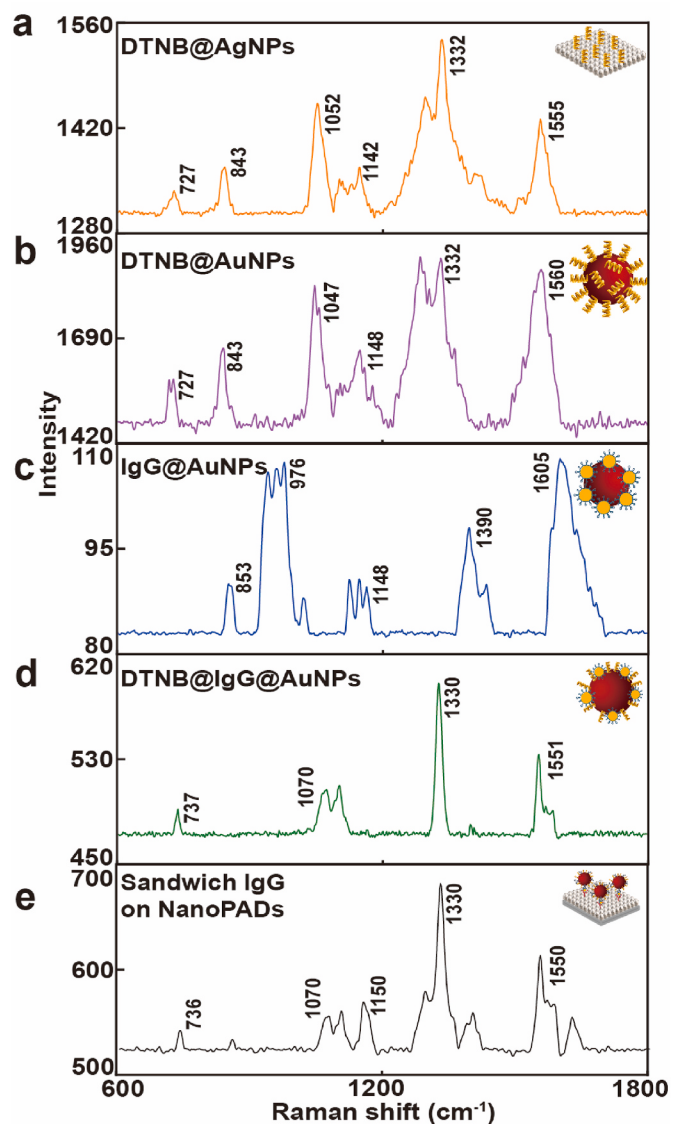


Fig. 3. The SERS spectra of DTNB and IgG. (a) The SERS spectrum of DTNB@AgNPs on NanoPADs. (b) The SERS spectrum of DTNB@AuNPs. (c) The SERS spectrum of IgG@AuNPs. (d) The SERS spectrum of DTNB@IgG@AuNPs. (e) The SERS spectrum of IgG sandwich immunoassay on NanoPADs (Capture: IgG capture antibody; SERS tags: DTNB@anti-IgG@AuNPs; determinand: IgG).

molecules increased proportionally with the increment in rabbit IgG concentration. These spectra revealed all the prominent characteristic Raman bands of IgG at 750 cm^{-1} , 830 cm^{-1} , 1060 cm^{-1} , 1140 cm^{-1} , 1330 cm^{-1} , 1415 cm^{-1} and 1555 cm^{-1} . The concentration-dependent SERS spectrum was further evaluated by plotting the intensity at 1330 cm^{-1} against the logarithm of rabbit IgG concentration. The equation $y = 79\lg x + 72$ describes the concentration-dependent SERS intensity at this specific peak. Fig. 4b demonstrates a good linear relationship between SERS intensity and rabbit IgG concentration, exemplifying high reproducibility. It underscores the method's capacity to consistently achieve antigen detection sensitivity across a range of low to very low concentrations. Using the conventional calibration curve, the quantitative values of the respective biomarkers were determined based on the characteristic peak of the specific Raman reporter. Using pure BSA as the blank control, LOD was calculated to be 369 fg mL^{-1} , defined as the rabbit IgG concentration corresponding to the blank control intensity plus three times the standard deviation of the Raman intensity of the blank control. The error bars in the plot illustrate the

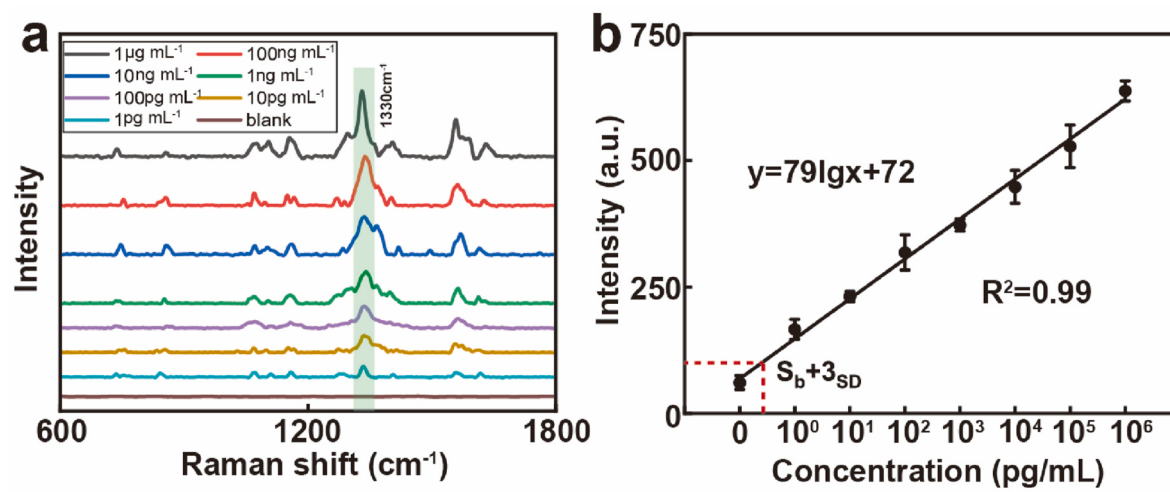


Fig. 4. SERS-based detection of IgG. (a) The SERS spectra of IgG at $1 \mu\text{g mL}^{-1}$ to 1 pg mL^{-1} concentrations. (b) Calibration of IgG at 1330 cm^{-1} ($n = 7$).

sample-to-sample variability in the SERS intensities. Without complementary antigens, washing effectively removes the DTNB-labeled AuNPs report probe from the immune substrate. Importantly, the blank control spectra demonstrated no evidence of non-specific binding between the report probe and the immune substrate. From these results, we proved the feasibility of this method in high selectivity and sensitivity of further GFAP SERS detection.

3.4. Optimization of the GFAP SERS immunoassay

The optimization of experimental conditions for the sandwich immunoassay aimed to determine the optimal antibody concentration for the assay while studying the Raman enhancement effects of these probes under the same protein concentration. In Fig. 5a, the Raman spectra of different concentrations of antibodies added to the SERS tags are depicted. For this experiment, various concentrations of GFAP antibodies were added to the AuNPs solution and incubated at room temperature for 2 h. The observed trend is clear: as the antibody concentration increased from $20 \mu\text{g mL}^{-1}$ to $100 \mu\text{g mL}^{-1}$, the Raman signal gradually intensified. This enhancement in Raman signal intensity can be attributed to the complete binding of antigen and antibody. However, at an antibody concentration of $200 \mu\text{g mL}^{-1}$, the Raman signal did not exhibit significant differences due to antibody saturation [57]. Based on these findings, the antibody concentration selected for this study is $100 \mu\text{g mL}^{-1}$.

Fig. 5b(i) and 5b(ii) show the SERS spectra of GFAP directly adsorbed on AuNPs, and sandwich immunoassay with Raman reporter DTNB,

respectively. The introduction of DTNB significantly enhances the detection sensitivity compared to direct GFAP detection. DTNB is commonly employed in immunoassays due to its facile functionalization and manipulation. Additionally, the inclusion of DTNB leads to a shift in the Raman peak of GFAP, possibly due to alterations in the distance between the molecule and the AuNPs surface. To demonstrate the specificity and selectivity of our method, we detected the GFAP protein in the presence of other similar neurological disease proteins, particularly other AD biomarkers, including P-tau and A β 42, which have similar functional group structures with GFAP [58,59]. In AD patients, concentrations of P-tau and A β 42, like GFAP, increase to a threshold level with the severity of AD, potentially interfering with GFAP detection. 61 pg mL^{-1} P-tau and 20 pg mL^{-1} A β 42 biomarkers, which were the threshold of AD [60,61], were added to GFAP protein at different concentrations, respectively. The observed increase in intensity at 1270 cm^{-1} , compared to the detection of only GFAP, is attributed to this peak being the highest characteristic peak of both P-tau and A β 42. Fig. 5c illustrates that there is no significant impact on the SERS characteristic peaks and intensity of GFAP by other proteins, thanks to the higher enhancement of the Raman reporter DTNB. This result underscores the effective and specific adsorption of the GFAP antigen and antibody. Furthermore, the GFAP group still exhibits detectable SERS characteristic peaks even in the presence of P-tau and A β 42 interference, demonstrating the applicability of the SERS immune substrate for humoral detection. These results established the ability of the proposed immunoassay to specifically and effectively detect target proteins.

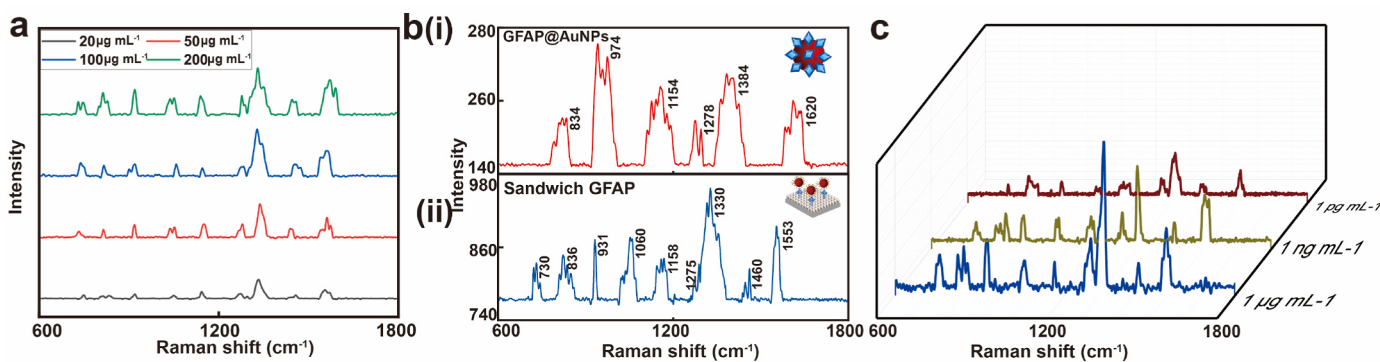


Fig. 5. Optimization of the GFAP SERS immunoassay. (a) The SERS spectra of different GFAP capture antibody amounts ranged from $20 \mu\text{g mL}^{-1}$ to $200 \mu\text{g mL}^{-1}$. (b) The SERS spectra of (i) GFAP@AuNPs and (ii) Sandwich GFAP immunoassay (Capture: GFAP capture antibody; SERS tags: DTNB@anti-GFAP@AuNPs; determinand: GFAP). (c) Specific Raman detection of GFAP in the presence of other AD biomarkers interference (P-tau and A β 42).

3.5. GFAP protein detection

Under the optimized conditions, the potential diagnostic value of this immunoassay was verified by testing GFAP in artificial serum. As shown in Fig. 6a, the SERS spectra for the detection of GFAP in artificial serum exhibit a concentration-dependent trend, ranging from $1 \mu\text{g mL}^{-1}$ to 1 pg mL^{-1} , with DTNB as the Raman reporter. The spectra exhibit prominent characteristic Raman bands of sandwich GFAP, with peaks at 730 cm^{-1} , 810 cm^{-1} , 856 cm^{-1} , 930 cm^{-1} , 1056 cm^{-1} , 1146 cm^{-1} , 1281 cm^{-1} , 1332 cm^{-1} , 1444 cm^{-1} and 1552 cm^{-1} . The SERS intensity shows a gradual decrease with an increasing dilution ratio. The intensity of the 1332 cm^{-1} peak, chosen due to its high sensitivity to GFAP concentration with minimal background noise, was used for analysis. The SERS peak intensity (y) versus the logarithm of GFAP concentration (x) was fitted using the equation $y = 137\lg x + 5$, yielding a relative coefficient R^2 of 0.99. In Fig. 6b, the calibration curve for GFAP detection is presented, and the LOD was calculated to be 150 fg mL^{-1} ($n = 7$). This LOD of our method is a notable improvement compared to the golden-standard LOD of ELISA detection ($10\text{--}600 \text{ ng mL}^{-1}$) [62]. The blank spectrum is determined using BSA ($1 \mu\text{g mL}^{-1}$). The error bars depicting GFAP at different concentrations demonstrate a consistent linear relationship between SERS intensity and GFAP concentration, indicating high reproducibility. Therefore, this strategy for detecting GFAP provides a simple and convenient tool with practical value for detecting GFAP. We further evaluated the stability of DTNB@anti-GFAP@AuNPs by testing SERS results after one week, two weeks and one month of storage, finding consistent results compared to the freshly prepared samples (Fig. S4). With the growth of storing time, the intensity of GFAP detection decreased slowly, and the noise of the characteristic peaks increased (between 1056 cm^{-1} and 1146 cm^{-1} peaks). Also, DTNB@anti-GFAP@AuNPs was still detectable after storing for one month under 4°C . The demonstrated specificity of this method holds significant practical implications for its application in complex biological systems.

Several factors contribute to this good performance. NanoPADs offer several advantages that contribute to their remarkable performance. Their highly integrated and simplified fabrication process minimizes pollution and the introduction of impurities, thus reducing interference. Additionally, NanoPADs' outstanding optical transparency and light reflection properties mitigate signal loss. The unique nanocellulose carboxyl structure of NanoPADs facilitates the uniform development of *in-situ* AgNPs. The selection of appropriate Raman reporter molecules enables straightforward single-step amplification. These combined advantages render the detection concept more accessible and adaptable to various analytes.

4. Conclusion

In this study, we have demonstrated a new platform for quantitatively detecting GFAP through the SERS-based immunoassay. Utilizing microfluidic technology, we devised a sandwich structure involving DTNB@anti-GFAP@AuNPs, and fixed it onto closed NanoPADs. This strategy afforded precise control over experimental conditions, leading to enhanced sensitivity compared to conventional SERS substrates. First, we verified the feasibility of the experimental design by detecting rabbit IgG antigens and achieved a LOD of 369 fg mL^{-1} . Second, GFAP, a potential biomarker for the early detection of AD, was used in this study. We optimized the experimental conditions to determine the amount of antibody for the immunoassay, and the GFAP detection antibody concentration was selected as $100 \mu\text{g mL}^{-1}$ for fabricating SERS tags. Finally, we established a calibration curve of GFAP concentration ranging from $1 \mu\text{g mL}^{-1}$ to 1 pg mL^{-1} and achieved a femtogram LOD (150 fg mL^{-1}), which is 20 times better than the other transparent SERS substrate (glass) and more suitable for early detection of AD. Our SERS-based immunoassay is a specific, cost-efficient, easy-to-operation, and sensitive method that provides new possibilities for detecting biomarkers. Our work lays the foundation for future SERS-based immunoassay of multiple biomarkers on NanoPADs for various diseases.

Author response

All the images/artwork/photos that appear in your manuscript and SI file were created by the authors of this manuscript.

CRediT authorship contribution statement

Wenwen Yuan: Writing – review & editing, Writing – original draft, Visualization, Methodology, Formal analysis, Data curation, Conceptualization. **Hang Yuan:** Writing – review & editing, Writing – original draft, Visualization, Methodology, Formal analysis. **Ruibing Li:** Writing – review & editing, Conceptualization. **Ruiqi Yong:** Writing – original draft, Visualization. **Ivona Mitrovic:** Project administration, Conceptualization. **Eng Gee Lim:** Writing – original draft, Project administration, Funding acquisition. **Sixuan Duan:** Writing – original draft, Visualization. **Pengfei Song:** Writing – review & editing, Writing – original draft, Visualization, Supervision, Funding acquisition, Conceptualization.

Declaration of competing interest

The authors declare that they have no known competing financial interests or personal relationships that could have appeared to influence

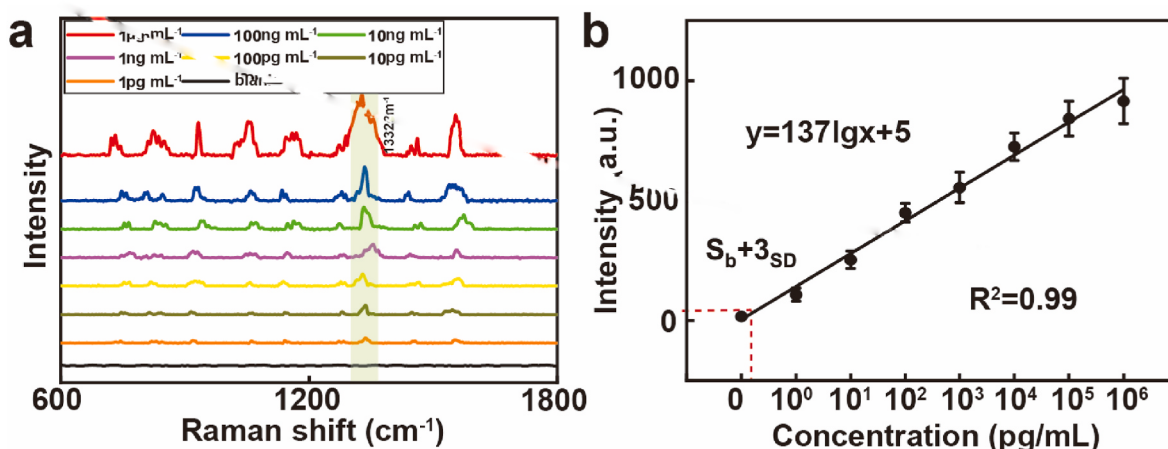


Fig. 6. SERS-based detection of GFAP. (a) The SERS spectrum of GFAP at $1 \mu\text{g mL}^{-1}$ to 1 pg mL^{-1} concentrations. (b) Calibration of GFAP at 1332 cm^{-1} ($n = 7$).

the work reported in this paper.

Data availability

Data will be made available on request.

Acknowledgment

The authors acknowledge the financial support from the programs of the Natural Science Foundation of the Jiangsu Higher Education (22KJB460033), Jiangsu Science and Technology Programme - Young Scholar (BK20200251), and XJTLU RDF projects (RDF-18-02-20, RDF-21-02-076). This work is also partially supported by the XJTLU AI University Research Centre, Jiangsu Province Engineering Research Centre of Data Science and Cognitive Computation at XJTLU, and the SIP AI innovation platform (YZCXPT2022103). The support from the State Key Laboratory for Manufacturing Systems Engineering via the open project (SKLMS2023019) and the Key Laboratory of Bionic Engineering, Ministry of Education at Jilin University (KF2023007), is also acknowledged.

Appendix A. Supplementary data

Supplementary data to this article can be found online at <https://doi.org/10.1016/j.aca.2024.342447>.

References

- [1] M. Citron, Alzheimer's disease: treatments in discovery and development, *Nat. Neurosci.* 5 (2002) 1055–1057.
- [2] K. Blennow, H. Hampel, M. Weiner, H. Zetterberg, Cerebrospinal fluid and plasma biomarkers in Alzheimer disease, *Nat. Rev. Neurol.* 6 (2010) 131–144.
- [3] R. Brookmeyer, E. Johnson, K. Ziegler-Graham, H.M. Arrighi, Forecasting the global burden of Alzheimer's disease, *Alzheimer's Dementia* 3 (2007) 186–191.
- [4] Alzheimer's Association, W. Thies, L. Bleiler, Alzheimer's disease facts and figures, *Alzheimer's Dementia* 9 (2013) 208–245, 2013.
- [5] K. Blennow, CSF biomarkers for mild cognitive impairment, *J. Intern. Med.* 256 (2004) 224–234.
- [6] G.M. McKhann, D.S. Knopman, H. Chertkow, B.T. Hyman, C.R. Jack, C.H. Kawas, W.E. Klunk, W.J. Koroshetz, J.J. Manly, R. Mayeux, R.C. Mohs, J.C. Morris, M. N. Rossor, P. Scheltens, M.C. Carrillo, B. Thies, S. Weintraub, C.H. Phelps, The diagnosis of dementia due to Alzheimer's disease: recommendations from the National Institute on Aging-Alzheimer's Association workgroups on diagnostic guidelines for Alzheimer's disease, *Alzheimer's Dementia* 7 (2011) 263–269.
- [7] S. Norton, F.E. Matthews, D.E. Barnes, K. Yaffe, C. Brayne, Potential for primary prevention of Alzheimer's disease: an analysis of population-based data, *Lancet Neurol.* 13 (2014) 788–794.
- [8] W. Pelkmans, M. Shekari, A. Brugulat-Serrat, G. Sánchez-Benavides, C. Minguillón, K. Fauria, J.L. Molinuevo, O. Grau-Rivera, A. González Escalante, G. Kollmorgen, M. Carboni, N.J. Ashton, H. Zetterberg, K. Blennow, M. Suárez-Calvet, J.D. Gispert, For the A. Study, Astrocyte biomarkers GFAP and YKL-40 mediate early Alzheimer's disease progression, *Alzheimer's Dementia* (2023).
- [9] X.-N. Shen, S.-Y. Huang, M. Cui, Q.-H. Zhao, Y. Guo, Y.-Y. Huang, W. Zhang, Y.-H. Ma, S.-D. Chen, Y.-R. Zhang, S.-F. Chen, K.-L. Chen, W. Cheng, C.-T. Zuo, L. Tan, D. Ding, Q. Dong, A. Jeromin, T.-C. Yen, J.-T. Yu, Plasma glial fibrillary acidic protein in the alzheimer disease continuum: relationship to other biomarkers, differential diagnosis, and prediction of clinical progression, *Clin. Chem.* 69 (2023) 411–421.
- [10] J.B. Pereira, S. Janelidze, R. Smith, N. Mattsson-Carlgren, S. Palmqvist, C. E. Teunissen, H. Zetterberg, E. Stomrud, N.J. Ashton, K. Blennow, O. Hansson, Plasma GFAP is an early marker of amyloid- β but not tau pathology in Alzheimer's disease, *Brain* 144 (2021) 3505–3516.
- [11] J. Simrén, H. Weninger, W.S. Brum, S. Khalil, A.L. Benedet, K. Blennow, H. Zetterberg, N.J. Ashton, Differences between blood and cerebrospinal fluid glial fibrillary Acidic protein levels: the effect of sample stability, *Alzheimer's Dementia* 18 (2022) 1988–1992.
- [12] A. Abdelhak, M. Foschi, S. Abu-Rumeileh, J.K. Yue, L. D'Anna, A. Huss, H. Tumani, Blood GFAP as an emerging biomarker in brain and spinal cord disorders, *Nat. Rev. Neurol.* 18 (2022) 158–172.
- [13] H.J. Butler, L. Ashton, B. Bird, G. Cinque, K. Curtis, J. Dorney, K. Esmonde-White, N.J. Fullwood, B. Gardner, P.L. Martin-Hirsch, M.J. Walsh, M.R. McAinch, N. Stone, F.L. Martin, Using Raman spectroscopy to characterize biological materials, *Nat. Protoc.* 11 (2016) 664–687.
- [14] E.C. Dreaden, A.M. Alkilany, X. Huang, C.J. Murphy, M.A. El-Sayed, The golden age: gold nanoparticles for biomedicine, *Chem. Soc. Rev.* 41 (2012) 2740–2779.
- [15] H. Zhu, Z. Fang, C. Preston, Y. Li, L. Hu, Transparent paper: fabrications, properties, and device applications, *Energ. Environ. Sci.* 7 (2013) 269–287.
- [16] M. Nogi, S. Iwamoto, A.N. Nakagaito, H. Yano, Optically transparent nanofiber paper, *Adv. Mater.* 21 (2009) 1595–1598.
- [17] N. Lavoine, I. Desloges, A. Dufresne, J. Bras, Microfibrillated cellulose – its barrier properties and applications in cellulosic materials: a review, *Carbohydr. Polym.* 90 (2012) 735–764.
- [18] X. Li, W. Ding, S. Wang, L. Yang, Q. Yu, C. Xiao, G. Chen, L. Zhang, S. Guan, D. Sun, Three-dimensional sulfated bacterial cellulose/gelatin composite scaffolds for culturing hepatocytes, *Cyborg. Bionic Syst.* 4 (2023) 0021.
- [19] F. Louis, M. Piantino, H. Liu, D.-H. Kang, Y. Sowa, S. Kitano, M. Matsusaki, Bioprinted vascularized mature adipose tissue with collagen microfibers for soft tissue regeneration, *Cyborg. Bionic Syst.* 2021 (2021) 1412542.
- [20] A. Dufresne, Nanocellulose: a new ageless bionanomaterial, *Mater. Today Off.* 16 (2013) 220–227.
- [21] F.J. Martin-Martinez, Designing nanocellulose materials from the molecular scale, *Proc. Natl. Acad. Sci. USA* 115 (2018) 7174–7175.
- [22] Z. Fang, H. Zhu, Y. Yuan, D. Ha, S. Zhu, C. Preston, Q. Chen, Y. Li, X. Han, S. Lee, G. Chen, T. Li, J. Munday, J. Huang, L. Hu, Novel nanostructured paper with ultrahigh transparency and ultrahigh haze for solar cells, *Nano Lett.* 14 (2014) 765–773.
- [23] L. Hu, G. Zheng, J. Yao, N. Liu, B. Weil, M. Eskilsson, E. Karabulut, Z. Ruan, S. Fan, J.T. Bloking, M.D. McGhee, L. Wågberg, Y. Cui, Transparent and conductive paper from nanocellulose fibers, *Energy Environ. Sci.* 6 (2013) 513–518.
- [24] H. Sehaqui, Q. Zhou, O. Ikkala, L.A. Berglund, Strong and tough cellulose nanopaper with high specific surface area and porosity, *Biomacromolecules* 12 (2011) 3638–3644.
- [25] W. Yuan, H. Yuan, K. Jiao, J. Zhu, E.G. Lim, I. Mitrovic, S. Duan, Y. Wang, S. Cong, C. Zhao, J. Sun, X. Liu, P. Song, Facile microembossing process for microchannel fabrication for nanocellulose-paper-based microfluidics, *ACS Appl. Mater. Interfaces* 15 (2023) 6420–6430.
- [26] W. Yuan, H. Yuan, S. Duan, R. Yong, J. Zhu, E.G. Lim, I. Mitrovic, P. Song, Microembossing: a convenient process for fabricating microchannels on nanocellulose paper-based microfluidics, *J. Vis. Exp.* 200 (2023) e65965.
- [27] Z. Cheng, N. Choi, R. Wang, S. Lee, K.C. Moon, S.-Y. Yoon, L. Chen, J. Choo, Simultaneous detection of dual prostate specific antigens using surface-enhanced Raman scattering-based immunoassay for accurate diagnosis of prostate cancer, *ACS Nano* 11 (2017) 4926–4933.
- [28] L. Chen, B. Ying, P. Song, X. Liu, A nanocellulose-paper-based SERS multiwell plate with high sensitivity and high signal homogeneity, *Adv. Mater. Interfac.* 6 (2019) 1901346.
- [29] J. Kim, C. Jo, W.-G. Lim, S. Jung, Y.M. Lee, J. Lim, H. Lee, J. Lee, W.J. Kim, Programmed nanoparticle-loaded nanoparticles for deep-penetrating 3D cancer therapy, *Adv. Mater.* 30 (2018) 1707557.
- [30] S.-E. Kim, B.-R. Lee, H. Lee, S.D. Jo, H. Kim, Y.-Y. Won, J. Lee, Near-infrared plasmonic assemblies of gold nanoparticles with multimodal function for targeted cancer theragnosis, *Sci. Rep.* 7 (2017) 17327.
- [31] Z. Rong, R. Xiao, S. Xing, G. Xiong, Z. Yu, L. Wang, X. Jia, K. Wang, Y. Cong, S. Wang, SERS-based lateral flow assay for quantitative detection of C-reactive protein as an early bio-indicator of a radiation-induced inflammatory response in nonhuman primates, *Analyst* 143 (2018) 2115–2121.
- [32] P. Zhao, H. Li, D. Li, Y. Hou, L. Mao, M. Yang, Y. Wang, A SERS nano-tag-based magnetic-separation strategy for highly sensitive immunoassay in unprocessed whole blood, *Talanta* 198 (2019) 527–533.
- [33] W.Y. Lim, C.H. Goh, T.M. Thevarajah, B.T. Goh, S.M. Khor, Using SERS-based microfluidic paper-based device (μ PAD) for calibration-free quantitative measurement of AMI cardiac biomarkers, *Biosens. Bioelectron.* 147 (2020) 111792.
- [34] J.J.S. Rickard, V. Di-Pietro, D.J. Smith, D.J. Davies, A. Belli, P.G. Oppenheimer, Rapid optofluidic detection of biomarkers for traumatic brain injury via surface-enhanced Raman spectroscopy, *Nat. Biomed. Eng.* 4 (2020) 610–623.
- [35] Y. Wang, X. Zhang, G. Wen, A. Liang, Z. Jiang, Facile synthesis of a highly SERS active nanosilver sol using microwaves and its application in the detection of E. coli using Victoria blue B as a molecular probe, *Anal. Methods* 8 (2016) 4881–4887.
- [36] C. Wei, M. Li, X. Zhao, Surface-enhanced Raman scattering (SERS) with silver nano substrates synthesized by microwave for rapid detection of foodborne pathogens, *Front. Microbiol.* 9 (2018) 2857.
- [37] M. Green, F.M. Liu, SERS substrates fabricated by island lithography: the silver/pyridine system, *J. Phys. Chem. B* 107 (2003) 13015–13021.
- [38] A. Hakonen, M. Svedendahl, R. Ogier, Z.-J. Yang, K. Lodewijks, R. Verre, T. Shegai, P.O. Andersson, M. Käll, Dimer-on-mirror SERS substrates with attogram sensitivity fabricated by colloidal lithography, *Nanoscale* 7 (2015) 9405–9410.
- [39] T. Saito, S. Kimura, Y. Nishiyama, A. Isogai, Cellulose nanofibers prepared by TEMPO-mediated oxidation of native cellulose, *Biomacromolecules* 8 (2007) 2485–2491.
- [40] J. Song, N.L. Birbach, J.P. Hinestroza, Deposition of silver nanoparticles on cellulosic fibers via stabilization of carboxymethyl groups, *Cellulose* 19 (2012) 411–424.
- [41] W. Kim, Y.-H. Kim, H.-K. Park, S. Choi, Facile fabrication of a silver nanoparticle immersed, surface-enhanced Raman scattering imposed paper platform through successive ionic layer absorption and reaction for on-site bioassays, *ACS Appl. Mater. Interfaces* 7 (2015) 27910–27917.
- [42] G. Frens, Controlled nucleation for the regulation of the particle size in monodisperse gold suspensions, *Nat. Phys. Sci. (Lond.)* 241 (1973) 20–22.
- [43] B. Xue, Q. Yang, X. Zhai, Z. Li, G.Y. Chen, D. Zhang, X. Zhou, An AuNPs/mesoporous NiO/nickel foam nanocomposite as a miniaturized electrode for heavy metal detection in groundwater, *Engineering* (2022).

- [44] C.-C. Lin, Y.-M. Yang, Y.-F. Chen, T.-S. Yang, H.-C. Chang, A new protein A assay based on Raman reporter labeled immunogold nanoparticles, *Biosens. Bioelectron.* 24 (2008) 178–183.
- [45] M. Bruchez, M. Moronne, P. Gin, S. Weiss, A.P. Alivisatos, Semiconductor nanocrystals as fluorescent biological labels, *Science* 281 (1998) 2013–2016.
- [46] W.C.W. Chan, S. Nie, Quantum dot bioconjugates for ultrasensitive nonisotopic detection, *Science* 281 (1998) 2016–2018.
- [47] Chuanming Duan, M.E. Meyerhoff, Separation-free sandwich enzyme immunoassays using microporous gold electrodes and self-assembled monolayer immobilized capture antibodies, *Anal. Chem.* 66 (1994) 1369–1377.
- [48] J. Yakovleva, R. Davidsson, A. Lobanova, M. Bengtsson, S. Eremin, T. Laurell, J. Emnéus, Microfluidic enzyme immunoassay using silicon microchip with immobilized antibodies and chemiluminescence detection, *Anal. Chem.* 74 (2002) 2994–3004.
- [49] Y. Shang, S. Cai, Q. Ye, Q. Wu, Y. Shao, X. Qu, X. Xiang, B. Zhou, Y. Ding, M. Chen, L. Xue, H. Zhu, J. Zhang, Quantum dot nanobeads-labelled lateral flow immunoassay strip for rapid and sensitive detection of *Salmonella typhimurium* based on strand displacement loop-mediated isothermal amplification, *Engineering* 19 (2022) 62–70.
- [50] J. Ni, R.J. Lipert, G.B. Dawson, M.D. Porter, Immunoassay readout method using extrinsic Raman labels adsorbed on immunogold colloids, *Anal. Chem.* 71 (1999) 4903–4908.
- [51] X. Zhang, S. Liu, X. Song, H. Wang, J. Wang, Y. Wang, J. Huang, J. Yu, Robust and universal SERS sensing platform for multiplexed detection of Alzheimer's disease core biomarkers using PAapt-AuNPs conjugates, *ACS Sens.* 4 (2019) 2140–2149.
- [52] S.A. Akintelu, S.C. Olugbeko, A.S. Folorunso, A review on synthesis, optimization, characterization and antibacterial application of gold nanoparticles synthesized from plants, *Int. Nano Lett.* 10 (2020) 237–248.
- [53] C. Coman, L.F. Leopold, O.D. Rugină, L. Barbu-Tudoran, N. Leopold, M. Tofană, C. Socaciu, Green synthesis of gold nanoparticles by Allium sativum extract and their assessment as SERS substrate, *J. Nanoparticle Res.* 16 (2013) 2158.
- [54] M.N. Lund, C.P. Baron, 2 - protein oxidation in foods and food quality, in: L. H. Skibsted, J. Risbo, M.L. Andersen (Eds.), *Chem. Deterioration Phys. Instab. Food Beverages*, Woodhead Publishing, 2010, pp. 33–69.
- [55] Z. Wang, S. Zong, H. Chen, H. Wu, Y. Cui, Silica coated gold nanoaggregates prepared by reverse microemulsion method: dual mode probes for multiplex immunoassay using SERS and fluorescence, *Talanta* 86 (2011) 170–177.
- [56] Z.A. Combs, S. Chang, T. Clark, S. Singamaneni, K.D. Anderson, V.V. Tsukruk, Label-free Raman mapping of surface distribution of protein A and IgG biomolecules, *Langmuir* 27 (2011) 3198–3205.
- [57] D. Yu, Q. Yin, J. Wang, J. Yang, Z. Chen, Z. Gao, Q. Huang, S. Li, SERS-based immunoassay enhanced with silver probe for selective separation and detection of Alzheimer's disease biomarkers, *Int. J. Nanomed.* 16 (2021) 1901–1911.
- [58] L. Zhang, K. Cao, Y. Su, S. Hu, X. Liang, Q. Luo, H. Luo, Colorimetric and surface-enhanced Raman scattering dual-mode magnetic immunosensor for ultrasensitive detection of blood phosphorylated tau in Alzheimer's disease, *Biosens. Bioelectron.* 222 (2023) 114935.
- [59] Y. Zhou, J. Liu, T. Zheng, Y. Tian, Label-free SERS strategy for in situ monitoring and real-time imaging of A β aggregation process in live neurons and brain tissues, *Anal. Chem.* 92 (2020) 5910–5920.
- [60] N. Fandos, V. Pérez-Grijalba, P. Pesini, S. Olmos, M. Bossa, V.L. Villemagne, J. Doecke, C. Fowler, C.L. Masters, M. Sarasa, Plasma amyloid β 42/40 ratios as biomarkers for amyloid β cerebral deposition in cognitively normal individuals, *Alzheimer's Dementia: Diagn. Assess. Dis. Monit.* 8 (2017) 179–187.
- [61] L. Tariciotti, M. Casadei, L.S. Honig, A.F. Teich, G.M. McKhann II, G. Tosto, R. Mayeux, Clinical experience with cerebrospinal fluid A β 42, total and phosphorylated tau in the evaluation of 1,016 individuals for suspected dementia, *J. Alzheimers Dis.* 65 (2018) 1417–1425.
- [62] M. Albrechtse, E. Bock, Quantification of glial fibrillary acidic protein (GFAP) in human body fluids by means of ELISA employing a monoclonal antibody, *J. Neuroimmunol.* 8 (1985) 301–309.